Supplementary Methods, Figures, and Tables for "Low thermal inertia of carbonaceous asteroid Bennu driven by cracks observed in returned samples," by Ryan, A. J. et al. *Nature Communications*

Supplementary Methods

Homogenization of large aggregate samples for coordinated analysis

Two large aggregate samples consisting of an unsorted mixture of particles from coarse (0.5–5 mm) to fine (<100 µm) in size were processed via mechanical grinding. The primary objectives of this processing were to (1) crush the sample to reduce the particle size to mostly fines without sieving, (2) minimize both inorganic and organic contamination of the sample during processing and allocation, (3) increase the surface area of the sample powder to maximize the solvent extraction efficiency of soluble organic molecules, and (4) reduce compositional heterogeneity of the powder for better comparisons of the results from different subsamples as part of coordinated analysis.

OREX-800107-0 and OREX-800117-0 were 6.425 g and 1.288 g aggregates scooped from sample trays OREX-800013-0 and OREX-800005-0, respectively, consisting of material originally derived from within TAGSAM. Both samples were XCT-scanned under pristine conditions at NASA JSC before processing (Methods).

OREX-800107-0 was processed at NASA JSC as described in *1* and summarized here. The sample was processed under a laminar flow bench in a clean room using quart mortar and pestle sets. All glassware and tools directly contacting the samples were baked out at 500°C overnight in air. Although baked-out aluminum foil was used, the goal was to avoid any direct contact of the foil with the sample during processing to prevent contamination with Al. As a processing control, ~7 g of granular silica chips (Isomass Analytics, 0.85–1.7 mm) heated at 500°C overnight was carried through the same steps as the Bennu aggregate.

Prior to powdering, a ~2 mm diameter, 8 mg particle (OREX-803203-0) was removed from the sample with stainless steel tweezers and sealed inside a glass concavity slide. ~2 g of the Bennu aggregate at a time was crushed to a fine powder while turning the mortar in the opposite direction as pestle movement. Powdering was done in cycles (not continuously) to minimize frictional heating. Two small particles that escaped the mortar during crushing and landed on clean Al foil were transferred with tweezers to a concavity slide (OREX-803204-0; 0.4 mg). The aggregate powder was then transferred from the mortar to the original glass container using a quartz funnel by scraping the interior of the mortar with the end of a glass pipet. The glass container with Bennu powder was re-sealed in air with the Viton cap and metal crimp, sealed inside a Teflon bag, and then analyzed by XCT at NASA JSC (Methods). Several fines from spillage too small to be collected with tweezers were collected from the foil by pressing against a carbon stub for scanning electron microscopy at JSC (OREX-800107-112). The mortar and pestle sets containing the Bennu aggregate (OREX-800107-100) and quartz powder residues were sealed in Teflon bags for later analysis.

The sample was weighed immediately before crushing and again after the post-crushing XCT scan, giving masses of 6.41320 g and 6.46184 g. The ~0.8% increase in mass is attributed to water absorption in air, which was not observed in the crushed silica control sample. Based on the difference between the pre- and post-crush mass of the fused silica, ~0.9% of the original mass could not be recovered from the mortar and pestle. The total X-ray dose of ~82 Gy applied to OREX-800107-0 sample during the XCT scans, calculated using the method of *2*, should not have led to any changes to the organic composition of the sample, based on previous XCT tests with the Murchison carbonaceous chondrite at a higher dose[1,3].

The homogenized powder of OREX-800107-0 and silica powders were transferred to glass concavity slides or screw-capped glass vials using the end of a glass pipet in the HEPA-filtered flow bench, weighed, and sealed inside a Teflon bag for eventual distribution. Between each transfer, the original glass container was tilted and rotated to mix the sample.

The aggregate sample OREX-800117-0 was processed at Lawrence Livermore National Laboratory. The full sample was homogenized in a mortar and pestle that had been cleaned three times successively with quartz sand, MQ water, 2N HCl, and methanol. The grinding procedure was similar to that described above for OREX-800107-0. The homogenized sample was divided into multiple aliquots to ship to various groups. A quartz sand sample was crushed in parallel as a control.

Supplementary Figures and Tables

Supplementary Table 1. Lock-in thermography thermal diffusivity and calculated thermal inertia. Results are reported as the average and associated error of the solutions across all azimuthal angles for a given measurement position, and the maximum and minimum solutions, which each come from a specific azimuthal direction. Measurement positions correspond to those shown in Fig. 1. Mean sample temperature measurement and measurement frequency are provided for each measurement.

Measure-ment position	Sample temperature (°C)	Frequency (Hz)	Mean sampling depth (µm)	Mean diffusivity ± 1-σ (10^{-7} m^2/s)	Maximum diffusivity (10^{-7} m^2/s)	Minimum diffusivity (10^{-7} m^2/s)	Mean thermal inertia ± 1-σ ($J\ m^{-2}\ K^{-1}\ s^{-½}$)	Maximum thermal inertia ($J\ m^{-2}\ K^{-1}\ s^{-½}$)	Minimum thermal inertia ($J\ m^{-2}\ K^{-1}\ s^{-½}$)
OREX-800118-0 (hummocky)									
1	31.2	2	340	1.8±0.6	3.1	1.1	550±90	720	430
1	31.7	4	250	1.9±0.6	3.7	1.1	570±90	790	430
2	32.6	0.5	680	1.8±0.7	2.6	0.9	550±110	660	390
2	33.0	4	220	1.5±0.9	2.7	0.6	500±160	680	320
4	33.0	20	140	2.9±0.6	3.5	2.5	700±70	770	650
7	33.4	0.5	840	2.8±1.4	4.5	1.4	690±180	870	490
7	33.6	4	310	3.0±0.8	4.4	1.9	710±100	860	570
8	32.5	0.5	890	3.1±1.2	4	1.6	720±140	820	520
8	33.1	4	340	3.7±0.8	5.4	2.3	790±90	960	620
9	33.4	0.5	780	2.4±1.1	4.2	0.8	640±150	840	370
9	32.7	4	350	3.9±1.4	5.6	2.7	810±150	970	680
10	30.6	0.5	710	2.0±1.8	3.4	0.6	580±310	760	320
10	30.0	4	270	2.3±1.4	4.1	1.2	620±200	830	450
11	33.8	0.5	780	2.4±1.2	4.8	0.4	640±170	900	260
11	33.0	4	270	2.3±0.9	4.3	0.8	620±130	850	370
12	33.3	20	140	3.1±1.1	4.6	2	720±130	880	580
12	34.7	40	100	3.1±0.7	4.7	2.5	730±80	890	650
OREX-803009-102 (angular)									
1	44.1	20	151	3.6±0.4	4	2.7	820±50	870	710
3	44.3	40	111	3.9±1.3	4.3	3.3	860±150	900	790
4	42.6	20	156	3.8±0.3	4.2	3.3	840±30	890	790
6	41.3	20	151	3.6±0.3	4.2	2.8	820±30	880	720
OREX-800055-7 (angular)									
1	46.7	4	352	3.9±0.5	4.5	3	920±60	990	810
2	47.7	4	339	3.6±0.4	4.8	3.2	880±50	1020	830
3	47.1	4	357	4.0±0.5	4.4	3.5	930±40	980	870
4	51.0	20	158	3.9±0.3	4.2	3.6	920±60	960	890
OREX-800055-8 (angular)									
1	53.6	40	107	3.6±0.3	4.1	2.9	890±40	950	800
2	52.6	40	110	3.8±0.3	5.7	3.5	920±40	1120	880
3	55.9	40	110	3.8±0.5	4.7	3	920±60	1020	820
4	40.0	20	164	4.2±0.4	4.7	4	940±40	1000	920

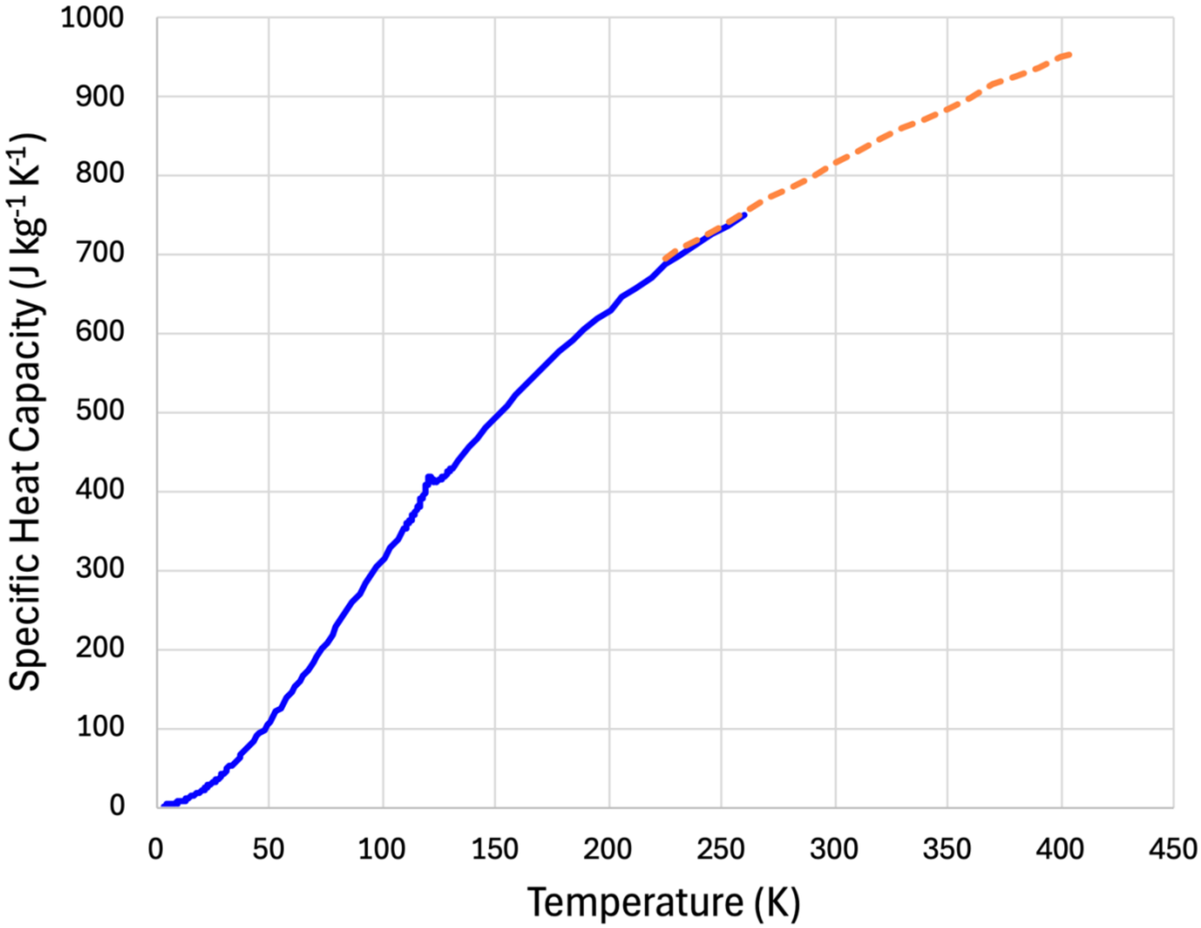

Supplementary Figure 1. Specific heat (c_p) of Bennu aggregate powder measured from 3 to 405 K. DSC, differential scanning calorimetry in solid blue; LTC, low-temperature relaxation calorimetry in dashed orange (Methods). Uncertainty decreases approximately linearly from ~8% to 1% between 3 K and 100 K and is ~1% above 100 K.

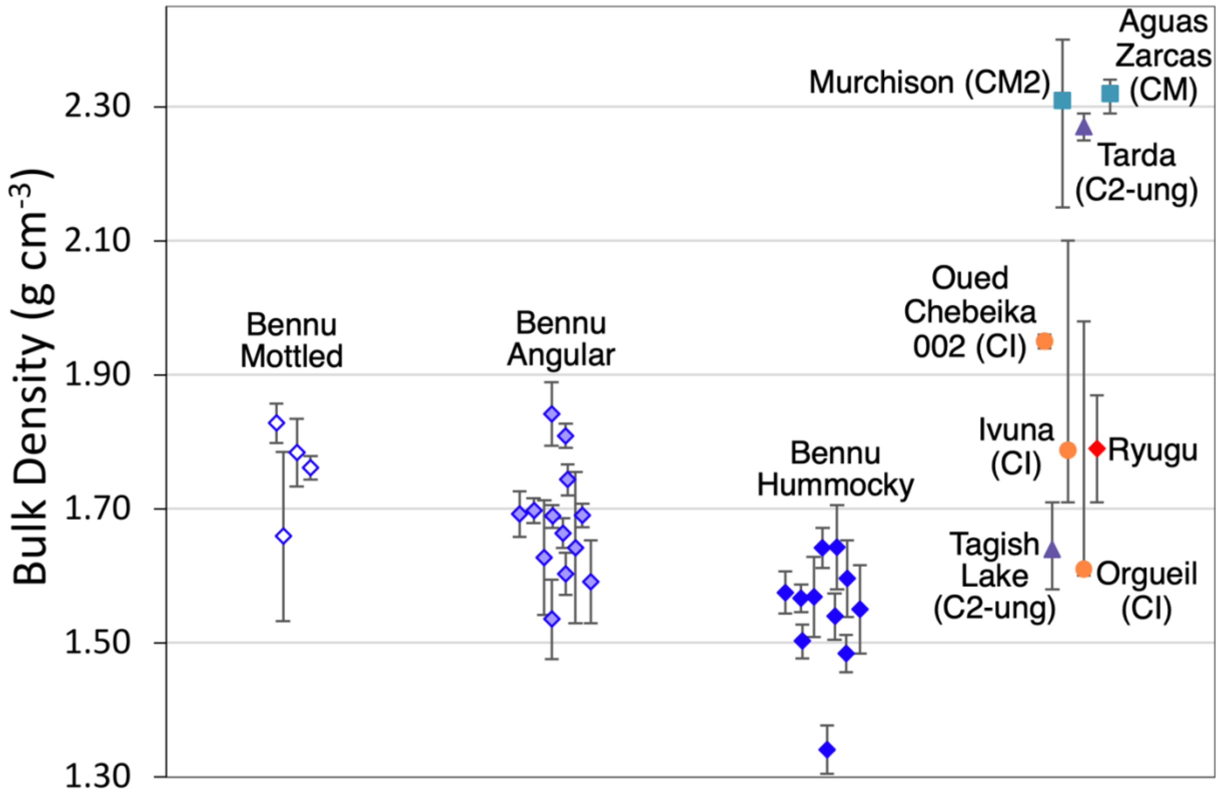

Supplementary Figure 2. Bulk density values for large (>50 mg) Bennu particles within the mottled, angular, and hummocky categories. Ryugu samples and possible meteorite analogs are shown for comparison. Data sources provided in Supplementary Table 2.

Supplementary Table 2. Densities of Bennu samples, Ryugu samples, and meteorites. The volume-weighted average density of meteorites with multiple specimens is denoted by the absence of a mass value. The classification of particles (mottled, angular, or hummocky) is based on external morphology and apparent brightness, as previously described[4,5]. Samples denoted with an asterisk (*) were not included in Supplementary Figure 2 due to their very small size.

Bennu Samples						
Sample ID	**Mass (g)**	**Type**	**SLS density (g cm^{-3})**	**XCT density (g cm^{-3})**	**Density uncertainty**	**Reference**
OREX-800014-0	6.236	Mottled	1.761		0.02	*4*
OREX-800016-0	1.183	Angular	1.697		0.02	this work
OREX-800017-0	2.042	Angular	1.690		0.02	*4*
OREX-800018-0	2.896	Angular	1.809		0.02	this work
OREX-800019-0	2.251	Angular	1.689	1.696	0.02	SLS: *4*; XCT: this work
OREX-800020-0	0.576	Angular	1.66		0.02	*4*
OREX-800021-0	0.592	Hummocky	1.57	1.59	0.02	SLS: *4*; XCT: this work
OREX-800023-0	0.399	Mottled	1.83	1.87	0.03	SLS: *4*; XCT: this work
OREX-800026-0	0.250	Hummocky	1.54		0.03	SLS: *4*; XCT: this work
OREX-800027-0	0.134	Hummocky		1.55	0.07	this work
OREX-800047-0	0.150	Angular		1.59	0.06	this work
OREX-800049-0	0.153	Hummocky		1.57	0.06	this work
OREX-800054-0	0.076	Angular		1.64	0.11	this work
OREX-800055-0	0.591	Angular	1.74	1.74	0.02	SLS: *4*; XCT: this work
*OREX-800055-7	0.003	Angular		*1.74*	*0.02*	Density assumed from parent OREX-800055-0
*OREX-800055-8	0.004	Angular		*1.74*	*0.02*	
OREX-800067-0	0.296	Angular	1.60	1.60	0.03	SLS: *4*; XCT: this work
OREX-800073-0	0.068	Mottled		1.66	0.13	this work
OREX-800087-0	0.372	Hummocky	1.50		0.03	*4*
OREX-800088-0	0.329	Hummocky	1.64	1.70	0.03	SLS: *4*; XCT: this work
OREX-800089-0	0.313	Hummocky	1.48	1.50	0.03	SLS: *4*; XCT: this work
OREX-800096-0	0.251	Mottled		1.78	0.05	this work
OREX-800097-0	0.168	Hummocky		1.60	0.06	this work
OREX-800098-0	0.150	Angular		1.54	0.06	this work
OREX-800099-0	0.152	Hummocky		1.64	0.06	this work
OREX-800118-0	0.04878	Hummocky		1.57	0.03	this work
OREX-800123-0	0.291	Angular		1.69	0.03	this work

OREX-800129-0	0.316	Angular		1.84	0.05	this work
OREX-800134-0	0.103	angular		1.63	0.09	this work
OREX-800141-0	0.279	Hummocky		1.34	0.04	this work
*OREX-803009-102	0.00187	Angular		1.6(3)	0.12	this work

<u>Other materials</u>

Name	Mass (g)	Type	Density (g cm^{-3})	Density uncertainty (g cm^{-3})	Reference
Ryugu	--	Asteroid sample	1.79	0.08	*6*
Ivuna	--	CI	1.787	+0.313, –0.077	*7*
Orgueil	--	CI	1.61	+0.37, –0.01	*7*
Murchison	--	CM2	2.31	+0.09,–0.16	*8*
Tagish Lake	--	C2-ungrouped	1.64	+0.07, –0.06	*9*
Aguas Zarcas	8.28	CM2	2.32	0.02	this work
Tarda	4.33	C2-ungrouped	2.27	0.02	this work
Oued Chebeika 002	2.59	CI	1.95	0.01	this work

Supplementary Table 3. **Abundance of individual mineral phases in powdered aggregate samples OREX-800107-103 and OREX-800117-108.** The abundances were measured via XRD (relative weight percentage), with the addition of undetected minor low-Ca pyroxene and amorphous organics based on previous Bennu sample analyses[4,10]. Grain density values assumed for the purpose of calculating the average grain density of each sample are from *11*, except dolomite is from *12*. Forsterite is assumed for olivine based on the bulk mineralogy of Bennu samples[4].

Phase	OREX-800107-103			OREX-800117-108			Assumed density (g cm^{-3})
	XRD relative wt%	Absolute wt%	vol%	XRD relative wt%	Absolute wt%	vol%	
Phyllosilicates (serpentines and smectites)	68.9	64.97	70.4	70.4	65.58	69.1	2.6±0.2
Magnetite, Fe_3O_4	11.9	11.22	6.1	9.1	8.48	4.5	5.2±0.02
Pyrrhotite, $Fe_{6.83}Ni_{0.17}S_8$	10.7	10.09	6.2	11	10.25	6.1	4.58±0.05
Pentlandite, $(Fe_{1-x}Ni_x)_9S_8$	3.9	3.68	2.0	2.6	2.42	1.3	5.08±0.1
Dolomite, $CaMg(CO_3)_2$	1.5	1.41	1.4	1.6	1.49	1.4	2.89±0.05
Calcite, $CaCO_3$	0.6	0.57	0.6	0.7	0.65	0.7	2.72±0.05
Olivine (predominantly forsterite, Mg_2SiO_4)	2.5	2.36	2.1	4.7	4.38	3.7	3.22±0.1
Low-Ca pyroxene	--	0.80	0.7	--	0.80	0.7%	3.3±0.1
Organic compounds	--	4.90	10.6	--	5.95	12.5%	1.3±0.3

Supplementary Table 4. Results from the thermal conductivity model for cracked samples. The length denotes the long axis (along which heat flow was simulated) of a cropped rectangular volume from the center of each sample's XCT dataset. These reduction factors account for both cracks and non-planar voids segmented from the XCT data.

Sample ID	Morphology	XCT Voxel size (µm)	Length (mm)	Conductivity reduction factor
OREX-800021-0	Hummocky	8.00	6.40	0.75
OREX-800088-0	Hummocky	8.50	6.21	0.59
OREX-800089-0	Hummocky	9.50	6.18	0.79
OREX-800097-0	Hummocky	6.50	4.88	0.60
OREX-800055-0	Angular	8.50	6.80	0.90
OREX-800123-0	Angular	6.25	5.00	0.90
OREX-800129-0	Angular	6.25	5.00	0.96

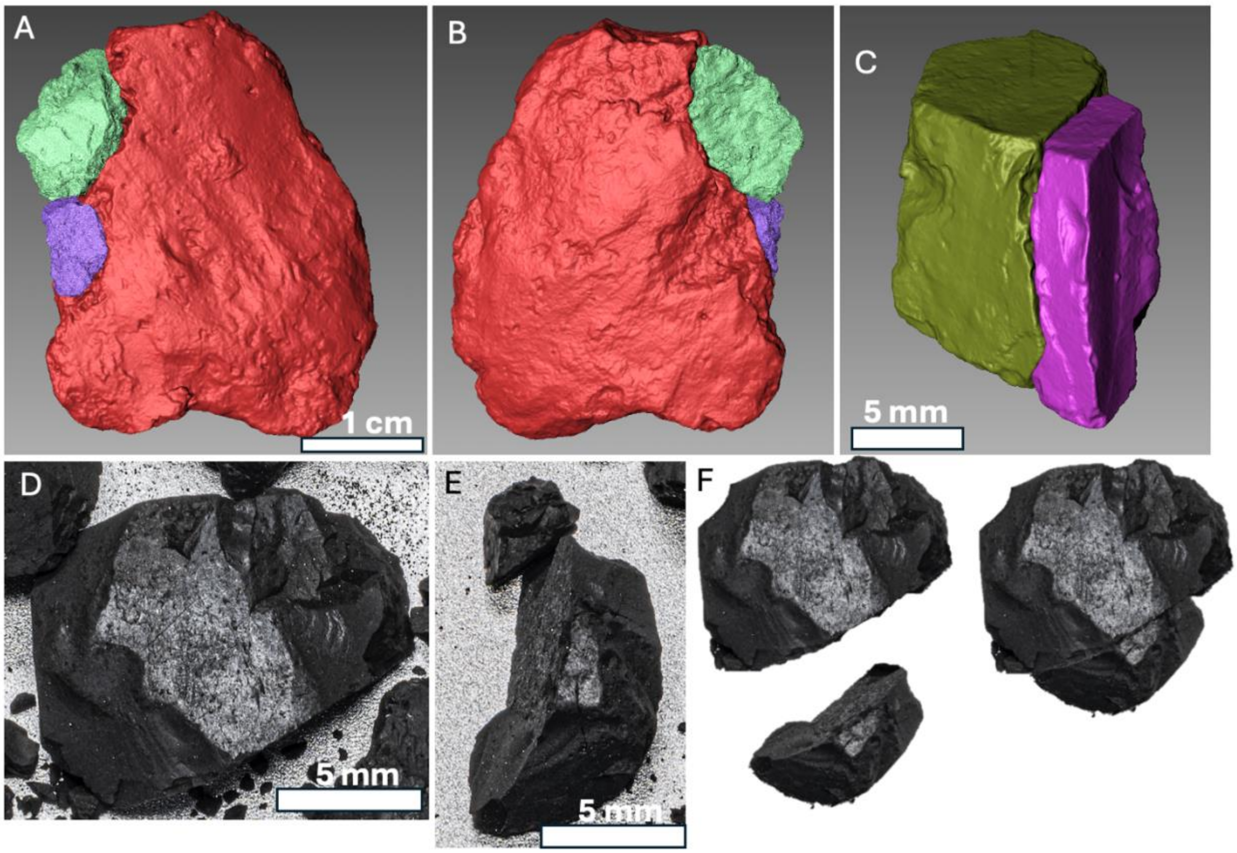

Supplementary Figure 3. Particles that can be geometrically reassembled like puzzle pieces. **(A, B)** 3D models (SLS, XCT) of three mottled particles, from largest to smallest: OREX-800014-0, OREX-800023-0, and OREX-800073-0. **(C)** 3D models (SLS, XCT) of two angular particles: OREX-800017-0 (larger) and OREX-800020-0 (smaller). **(D)** AIVA image of angular particle OREX-800016-0. **(E)** AIVA image of an unnamed particle within aggregate sample OREX-800010-0. **(F)** Photo-based assembly of OREX-800016-0 and the unnamed particle.

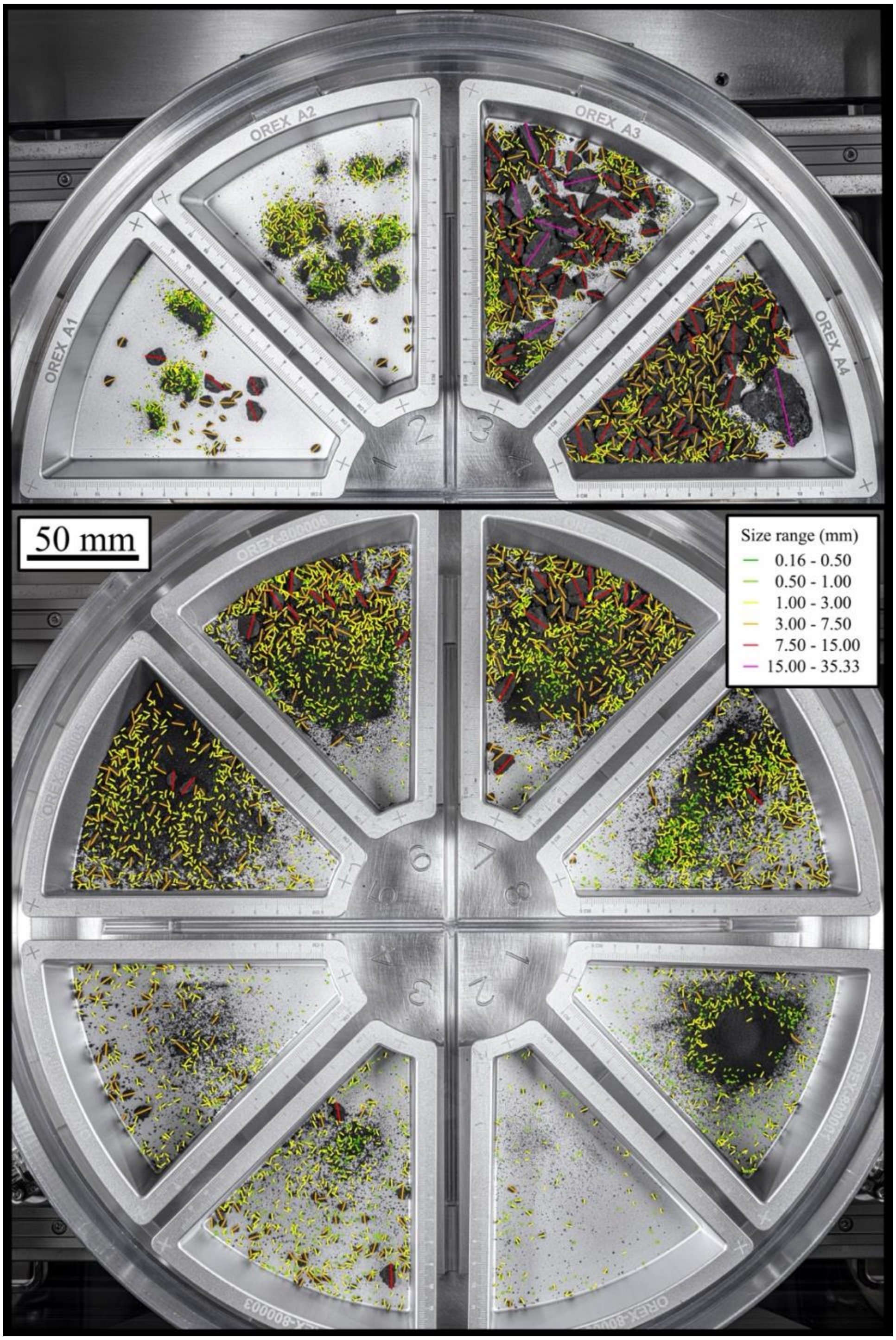

Supplementary Figure 4. **Particle long axes measured for the PSFD analysis, overlain on AIVA images of the complete sample collection from within TAGSAM.**

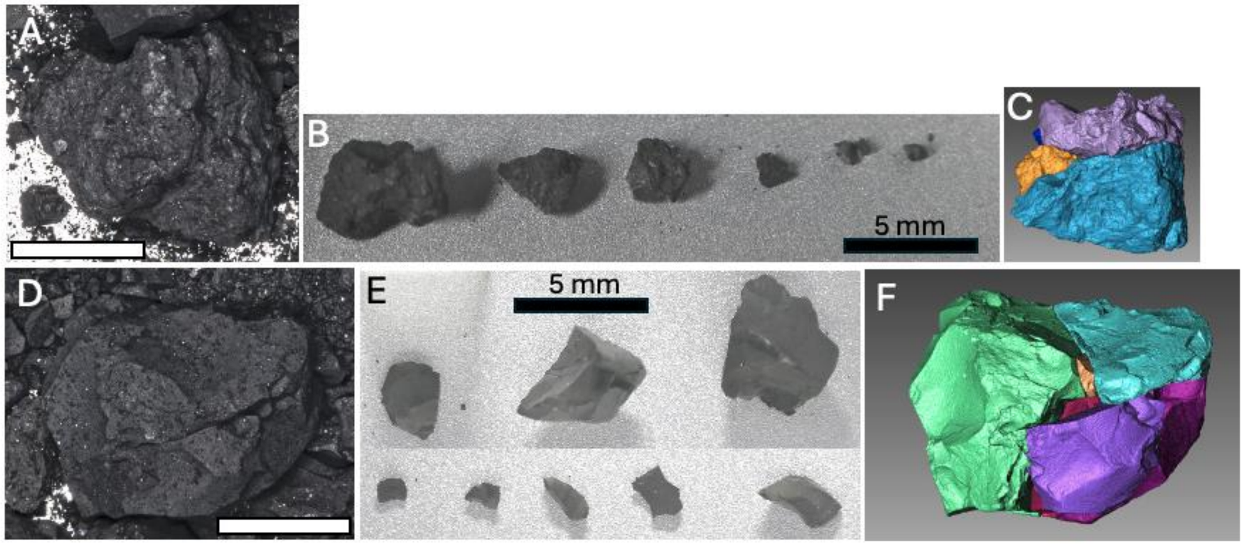

Supplementary Figure 5. Stones subjected to controlled splits. All scale bars are 5 mm. **(A)** AIVA image of hummocky sample OREX-800088-0. **(B)** Fragments produced from the split of OREX-800088-0. **(C)** Assembly of XCT models of large fragments of OREX-800088-0, excluding the largest fragment, which was set aside for thin sectioning to reduce the risk of breaking. **(D)** AIVA image of angular sample OREX-800055-0. **(E)** Fragments produced from the split of OREX-800055-0. **(F)** Assembly of XCT models of large fragments of OREX-800055-0.

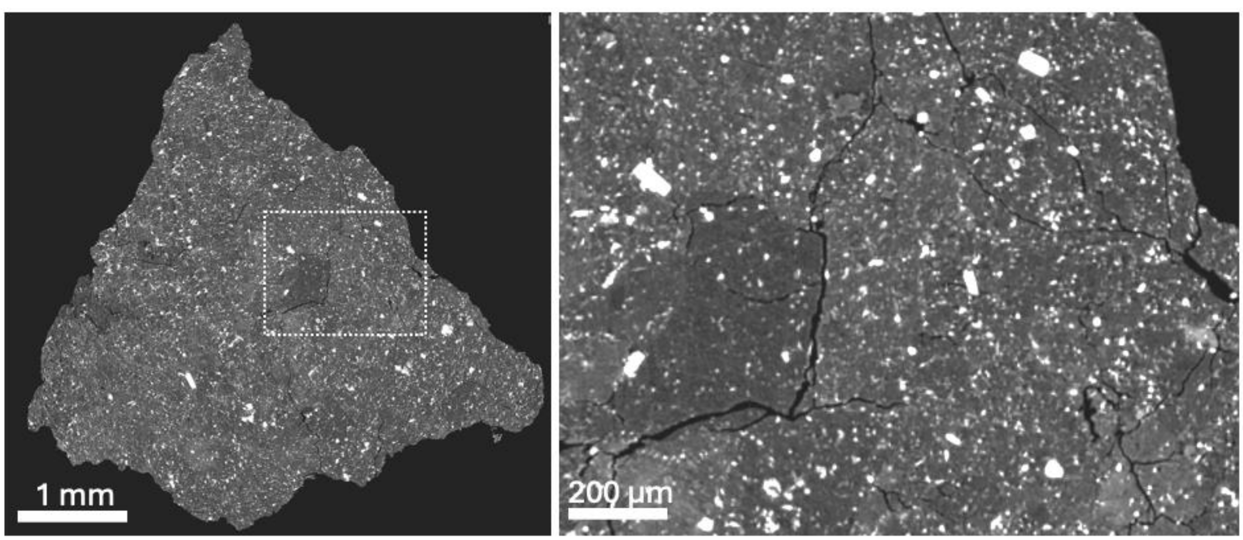

Supplementary Figure 6. XCT scan of Ryugu sample C0002. The dashed rectangle on the left corresponds to the zoomed view on the right showing details of internal crack networks.

Supplementary Table 5. Samples studied in this work, the laboratories where they were analyzed, the analytical techniques applied, and the DOIs of the resulting datasets, available via the Astromat repository (Astromat.org).

Sample ID	**Laboratory**	**Analysis**	**DOI(s)**
OREX-800014-0	Johnson Space Center	SLS	10.60707/64vm-zd18
OREX-800016-0	Johnson Space Center	SLS	10.60707/w2w2-0448
OREX-800017-0	Johnson Space Center	SLS	10.60707/fymn-n257
OREX-800018-0	Johnson Space Center	SLS	10.60707/pnfj-nc59
OREX-800019-0	Johnson Space Center	XCT	10.60707/nxge-6x60
	Johnson Space Center	SLS	10.60707/46vk-8e09
OREX-800020-0	Johnson Space Center	SLS	10.60707/c99t-qs13
OREX-800021-0	Johnson Space Center	XCT	10.60707/czsb-b064
	Johnson Space Center	SLS	10.60707/s4m1-4b95
OREX-800023-0	Johnson Space Center	XCT	10.60707/nptt-2x39
	Johnson Space Center	SLS	10.60707/3cqf-cm22
OREX-800027-0	Johnson Space Center	XCT	10.60707/140w-3640
OREX-800047-0	Johnson Space Center	XCT	10.60707/mjvq-aa31
OREX-800049-0	Johnson Space Center	XCT	10.60707/crnr-cf55
OREX-800054-0	Johnson Space Center	XCT	10.60707/6y35-r522
OREX-800055-0	Johnson Space Center	XCT	10.60707/2c1c-dz58 10.60707/8pbm-t622
	Johnson Space Center	SLS	10.60707/9tad-kq08
OREX-800055-7	Johnson Space Center	XCT	10.60707/8pbm-t622
	Nagoya University	LIT	10.60707/1csa-d407 10.60707/5jq4-e606 10.60707/zzzf-rk04 10.60707/j02p-f160
OREX-800055-8	Johnson Space Center	XCT	10.60707/8pbm-t622
	Nagoya University	LIT	10.60707/nmxa-bq43 10.60707/61fs-f092 10.60707/tnwv-xw63 10.60707/0n7w-m432
OREX-800055-9	Arizona State University	Nanoindentation	10.60707/66yd-4x39 10.60707/4fza-xy39 10.60707/0rhc-vr50 10.60707/rv6v-qs19 10.60707/dkan-8a54
OREX-800067-0	Johnson Space Center	XCT	10.60707/hvs8-a166
	Johnson Space Center	SLS	10.60707/dc7d-1949
OREX-800073-0	Johnson Space Center	XCT	10.60707/brk7-px44
OREX-800088-0	Johnson Space Center	XCT	10.60707/8w70-4b88

			10.60707/e4ys-8z20
	Johnson Space Center	SLS	10.60707/c2ga-7937
OREX-800088-5	Arizona State University	Nanoindentation	10.60707/v0a3-rz51 10.60707/g82j-ep03 10.60707/qck4-vj80
	Johnson Space Center	XCT	10.60707/e4ys-8z20
OREX-800089-0	Johnson Space Center	XCT	10.60707/3ds1-5396
	Johnson Space Center	SLS	10.60707/a3qn-ak31
OREX-800096-0	Johnson Space Center	XCT	10.60707/5dz0-7d81
OREX-800097-0	Johnson Space Center	XCT	10.60707/z0gq-5c10
OREX-800098-0	Johnson Space Center	XCT	10.60707/zvgn-8178
OREX-800099-0	Johnson Space Center	XCT	10.60707/5kkn-q343
OREX-800107-0	Johnson Space Center	XCT	10.60707/jnv8-1e46
OREX-800107-103	Natural History Museum of London	XRD	10.60707/w1v8-fs59
OREX-800107-104	Boston College	Heat Capacity	10.60707/zmnw-pj79
OREX-800117-0	Johnson Space Center	XCT	10.60707/zsgj-ed85
OREX-800117-108	Natural History Museum of London	XRD	10.60707/99k7-0y83
OREX-800118-0	Johnson Space Center	XCT	10.60707/xe71-ec20
	Univ. Texas at Austin	XCT	10.60707/zv0z-rb05 10.60707/41rq-gt37 10.60707/ye64-yn57
	Nagoya University	LIT	10.60707/a7ah-6540
OREX-800123-0	Johnson Space Center	XCT	10.60707/5m56-kv71
OREX-800129-0	Johnson Space Center	XCT	10.60707/dnfj-mf92
OREX-800134-0	Johnson Space Center	XCT	10.60707/z4yp-y044
OREX-800141-0	Johnson Space Center	XCT	10.60707/c8n6-t311
OREX-803009-102	University of Arizona	XCT	10.60707/w3st-m862
	Nagoya University	LIT	10.60707/8ybe-rc54 10.60707/3fa1-3w46 10.60707/zqkp-g646
OREX-803224-0	Nagoya University	DSC	10.60707/ja51-pz63 10.60707/rd8a-6z91
Sample trays (OREX-800001-0 to OREX-800008-0, OREX-800010-0 to OREX-800013-0)	Johnson Space Center	AIVA	10.60707/ek2k-3171 10.60707/7fk7-4x67
	INAF - Astronomical Observatory of Padova	PSFD	10.60707/ga4k-dn12

Supplementary References

1. Glavin, D. P. et al. The homogenization and sub-division of a large aggregate sample from asteroid Bennu for coordinated analyses. 56th Lunar and Planetary Science Conference, abstract 1079 (2025).
2. Friedrich, J. M. et al. Effect of polychromatic X-ray microtomography imaging on the amino acid content of the Murchison CM chondrite. *Meteorit. Planet. Sci.* **54**(1), 220–228 (2019).
3. Cody, G. D. et al. The nature of insoluble organic matter in Sutter's Mill and Murchison carbonaceous chondrites: Testing the effect of x-ray computed tomography and exploring parent body organic molecular evolution. *Meteorit. Planet. Sci.* **59**(1), 3–22 (2024).
4. Lauretta, D. S. & Connolly, H. C. Jr., et al. Asteroid (101955) Bennu in the laboratory: Properties of the sample collected by OSIRIS-REx. *Meteorit. Planet. Sci.* **59**, 2453–2486 (2024).
5. Connolly Jr., H. C. & Lauretta, D. S., et al. An overview of the petrography and petrology of particles from aggregate sample from asteroid Bennu. *Meteorit. Planet. Sci.* **60**(5), 979–996 (2025). https://doi.org/10.1111/maps.14335.
6. Nakamura T., Matsumoto M., Amano, K., Enokido., Y., Zolensky, M. E., et al. Formation and evolution of carbonaceous asteroid Ryugu: Direct evidence from returned samples. *Science* **379**, eabn8671 (2023). doi:10.1126/science.abn8671
7. Friedrich, J. M. et al. Physical properties, internal structure, and the three-dimensional petrography of CI chondrites. *Meteorit. Planet. Sci.* **60**(3), 632–645 (2025). https://doi.org/10.1111/MAPS.14320
8. Macke, R. J., Consolmagno, G. J. & Britt, D. T. Density, porosity, and magnetic susceptibility of carbonaceous chondrites. *Meteorit. Planet. Sci.* **46**, 1842–1862 (2011). https://doi.org/10.1111/j.1945-5100.2011.01298.x
9. Hildebrand, A. R. et al. The fall and recovery of the Tagish Lake meteorite. *Meteorit. Planet. Sci.* **41**(3), 407–431 (2006).
10. Foustoukos, D. I. et al. H, C, and N in samples with outer solar system heritage: Asteroid Bennu and the C2 ungrouped chondrites Tarda and Tagish Lake. 56th Lunar and Planetary Science Conference, abstract 1259 (2025).
11. Biele, J., Grott, M., Zolensky, M. E., Benisek, A. & Dachs, E. The specific heat of astro-materials: Review of Theoretical concepts, materials, and techniques. *Int. J. Thermophys.* **43**(9), 144, (2022). https://doi.org/10.1007/s10765-022-03046-5
12. Ahrens, T. J. *Mineral Physics and Crystallography: A Handbook of Physical Constants* (American Geophysical Union, 1995).